Additional Transition Line in Jammed Asymmetric Bidisperse Granular Packings

Juan C. Petit[,1] Nishant Kumar,[1] Stefan Luding,[2] and Matthias Sperl[1,3]

[1]*Institut für Materialphysik im Weltraum, Deutsches Zentrum für Luft- und Raumfahrt (DLR), 51170 Köln, Germany*
[2]*Multi-Scale Mechanics (MSM), Faculty of Engineering Technology, MESA+, University of Twente,*
PO Box 217, 7500 AE Enschede, The Netherlands
[3]*Institut für Theoretische Physik, Universität zu Köln, 50937 Köln, Germany*

We present numerical evidence for an additional discontinuous transition, upon compression, inside the jammed regime for an asymmetric bidisperse granular packing. This additional transition line separates jammed states with networks of predominantly large particles from jammed networks formed by both large and small particles, and the transition is indicated by a discontinuity in the number of particles contributing to the jammed network. The additional transition line emerges from the curves of jamming transitions and terminates in an end point where the discontinuity vanishes. The additional line is starting at a size ratio around $\delta = 0.22$ and grows longer for smaller δ. For $\delta \to 0$, the additional transition line approaches a limit that can be derived analytically. The observed jamming scenarios are reminiscent of glass-glass transitions found in colloidal glasses.

The jamming transition at packing fraction ϕ_J in granular matter is indicated by a discontinuous jump in the number of contacts per particle [1–6]. For frictionless monodisperse packings, that value is close to $\phi_J \approx 0.64$ in 3D [5,7]. To suppress crystallization, bidisperse packings are introduced where ϕ_J can be tuned to higher values by varying the size ratio δ and volume concentration of small particles X_S [8–12]. Such mixtures are also relevant for industrial processes since mechanical properties of bidisperse packings such as bulk modulus and wave speed can be controlled [13].

While the dependence of the jamming density on δ and X_S has been studied previously [8–12], a better understanding of jammed states in highly asymmetric bidisperse mixtures for extremely low X_S is intended here. For example, previous works have assumed that the jammed structure of a bidisperse packing is formed by the equal contribution of both large and small particles since both species jam simultaneously at ϕ_J [9–11]. This is true above certain values of δ and X_S, since then the particle sizes are similar enough that both species follow the same behavior. However, for lower values of δ and X_S, each component behaves differently when approaching jamming, which suggests a potential decoupling in the jamming in the binary system. Indeed, it has been recently demonstrated in Ref. [8] that the jammed structure of an asymmetric

bidisperse system evolves from a small-sphere rich to a small-sphere poor structure. Such behavior is marked by an abrupt drop in the number of small particles contributing to the jammed structure at a specific X_S, while the rest of the small particles remain without contacts.

The recent works cited above indicate that, in principle, two different pathways to jamming need to be distinguished for small δ: one driven by predominantly large particles and one driven by both species together. It is the aim of this Letter to demonstrate explicitly that such distinction can be made rigorous by an analysis of the partial contact numbers between particles of different species. This leads to the identification of an additional transition between different jammed states for $X_S < X_S^*(\delta)$ for $\delta \leq \delta^*$. The transition diagram for that scenario is shown in Fig. 1 and shall be elaborated on below. In the following, the simulation method shall be explained, followed by the analysis and discussion of the results; the results are rationalized theoretically and put into context with scenarios found in glasses in the Conclusion.

Simulations using the 3D discrete element method are performed with the software MercuryDPM [13,14]. Bidisperse packings are formed by $N = 6000$ particles, where a number of large N_L and small N_S particles with radius r_L and r_S are considered, respectively. Each packing is characterized by the size ratio, $\delta = r_S/r_L$, and the concentration of small particles, $X_S = N_S \delta^3 / (N_L + N_S \delta^3)$, as well as the overall packing fraction ϕ (see Supplemental Material, Sec. I for further details [15]). We restrict ourselves to the isotropic deformation and to the linear contact model without any friction between particles [16,17]. Thus, we exclude all the nonlinearities present in the system due to contact models
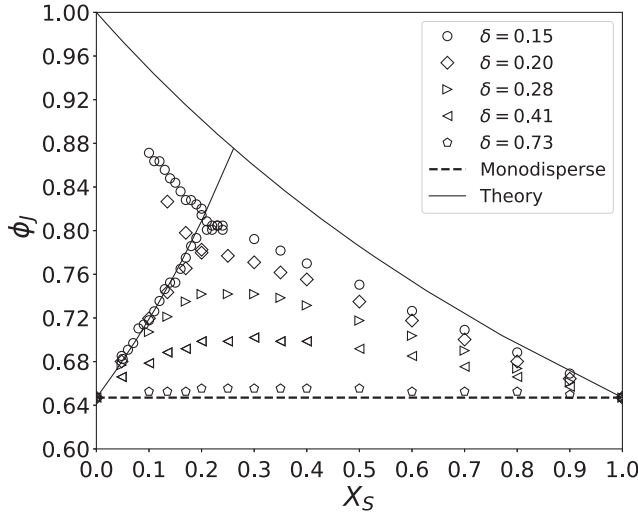
FIG. 1. Jamming density ϕ_J as a function of the volume concentration of small particles X_S for different values of the size ratio δ. The extreme X_S values (zero and one) correspond to monodisperse systems where $\phi_J \approx 0.645$ indicated by the dashed horizontal line. Solid lines represent the result of Eq. (1).

and analyze the effect of the size ratio and concentration of small particles at jamming. Each bidisperse packing characterized by the parameters (δ, X_S) is created and further compressed using an unique, well-defined protocol [16,18]. ϕ_J for each configuration is determined at the point where the partial mean contact number exhibits a sharp decay. The values of ϕ_J as a function of X_S for different δ are shown in Fig. 1.

For a particular $\delta = 0.15$, the jamming density increases with X_S up to a maximum value occurring at $X_S^*(0.15) \approx 0.21$, then decreases for larger values. Along the increasing transition line, jamming is driven by the force network created by the large particles, since most of the small ones remain without or with only few contacts in the cages formed by the large ones. This is confirmed when looking at Figs. 2(a) and 2(c), where mainly large particles are carrying the load in the jammed state. On the other hand, on the decreasing branch of ϕ_J for high X_S, small and large particles arrest simultaneously at the same density, see Figs. 2(b) and 2(d). However, for lower values of δ and X_S, a decoupling in the mean contact number Z between large and small particles is observed, see Fig. 2(a). Large particles arrest first at lower ϕ, while small ones remain without contacts. Making the packing denser, small particles exhibit an apparent jump in Z_{SS} and Z_{mix} [see Fig. 2(a)], indicating that a fraction of them start contributing in a discontinuous fashion to the already jammed structure of large ones. While the related conditions are certainly fulfilled by the setup of the simulation, simple Maxwell counting arguments or variations thereof [19] are not sufficient to explain the complex variation of contact numbers in that regime.

To corroborate the behavior observed in the Z_{SS}, in addition we have quantified the fraction of large n_L and
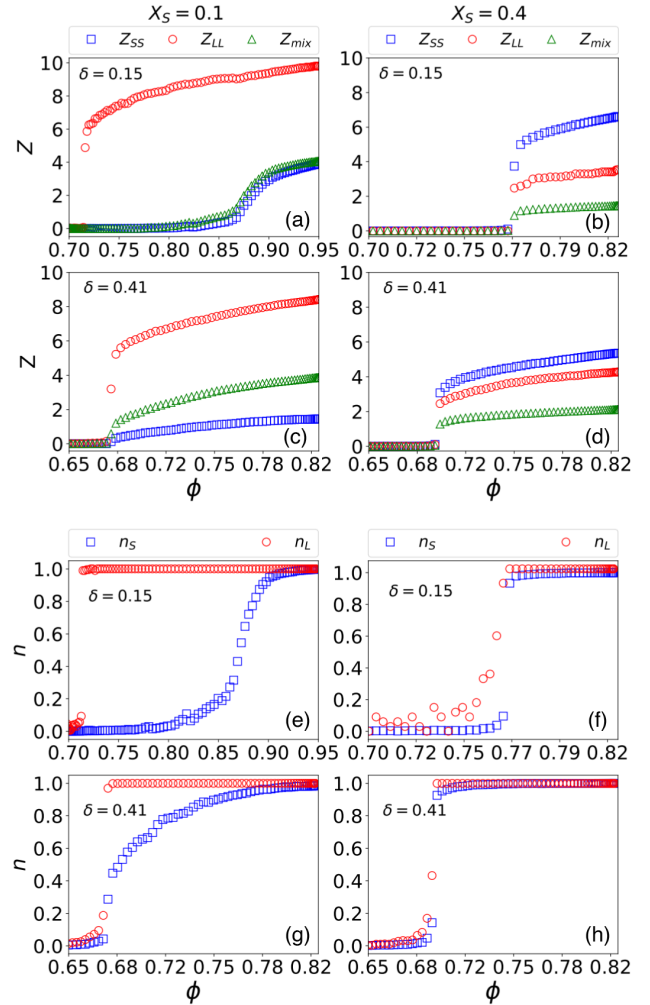

FIG. 2. (a)–(d) Mean contact number Z for each type of contact as a function of ϕ for four combinations of δ and X_S. Z_{nm} corresponds to the sum of contacts between particles of species n and m divided by total number of N particles, with $n, m \in [L, S]$. The analyzed data are taken along the decompression branch. Z_{mix} is defined as $Z_{\mathrm{mix}} = (Z_{LS} + Z_{SL})/N$. (e)–(h) Fractions of large n_L and small n_S particles contributing to the force network as a function of the packing fraction ϕ for two sets of (δ, X_S).

small particles n_S contributing to the force network as a function of ϕ shown in Figs. 2(e)–2(h). This quantity exhibits the additional jump more drastically compared to Z. A clear decoupling between n_L and n_S at lower δ and X_S can be seen in Fig. 2(e), while for higher values of δ, both sizes of particles contribute simultaneously to the jammed structure. Such decoupling indicates that a large amount of small particles are jammed discontinuously at higher densities, which resembles a similar behavior as by the large particles at low densities. To extract the precise value of the jamming density where n_S jumps for low X_S, we used the derivative of $\partial n_S / \partial \phi$ (see Supplemental Material [15], Sec. II). Figure 1 displays such values for $X_S < X_S^*(\delta) \approx 0.21$, indicated by the increasing line of densities for smaller X_S. Such a line extends the transitions
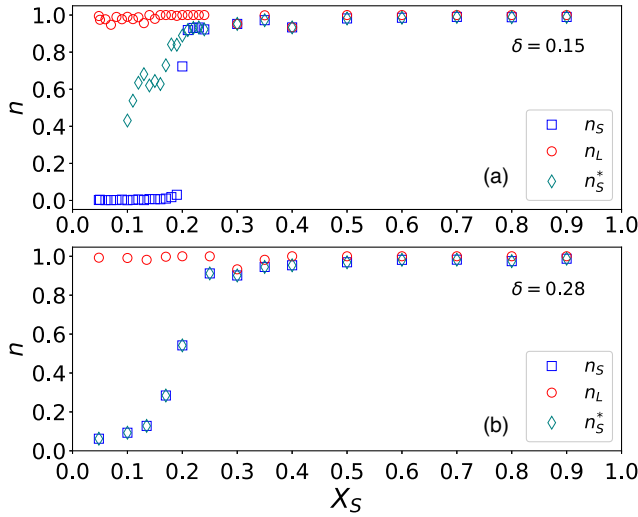
FIG. 3. Fraction of small n_S and large particles n_L contributing to the jammed structure as a function of the concentration X_S of small particles for (a) $\delta = 0.15$ and (b) $\delta = 0.28$. n_S^* represents the fraction of small particles along the additional line.

where both particle species are jammed into a regime of smaller X_S. For the larger $\delta = 0.20$, the additional line emerges from $X_S^*(0.20) \approx 0.18$. For $\delta = 0.15$ and 0.20, the packing fractions where the additional transition lines emerge are $\phi^* = 0.81$ and 0.79, respectively.

Except for the additional transition line, the results shown in Fig. 1 are quite similar to those previously found in experiments using glass beads [11] and in 3D simulations [9,10]. In those latter works, however, no additional line was identified. Recent work [8], which has studied the statistics of the small particles in the jammed structure of bidisperse systems in more detail, showed that indeed the fraction of small particles contributing to the jammed structure decays to small values for $X_S < X_S^*$, which becomes discontinuous as δ decreases. This allows one to make a distinction between two regimes: one where small particles contribute to the jammed network jointly with large ones ($X_S \geq X_S^*$) and the second one where only large particles contribute ($X_S < X_S^*$). We have found that, besides these two regimes, there is an additional line emerging at $X_S = X_S^*$. The additional line represents a jammed state ϕ_J, extending into higher densities and terminating in an end point $(X_S^\circ(\delta), \phi^\circ(\delta))$. The additional line starts emerging for $\delta < \delta^* = 0.22$ where the line's end point extends further to lower X_S as δ decreases.

The evolution of the fractions of small and large particles that contribute to the jammed structure, n_S and n_L, along the jamming lines elucidates the different nature of the transitions, i.e., by discussing the jump heights in these quantities as the jamming transition is crossed. These ratios are shown in Fig. 3 for two representative values of δ. Here, we extracted n_S and n_L from the points where the large-particle contribution jumps and n_S^* from those where the small-particle contribution jumps. The existence of the

additional transition line is now manifested in the cases where n_S^* splits from n_S, see Fig. 3(a) at low X_S. Close to the crossing point where the additional transition line emerges, the difference between n_S and n_S^* is largest. For lower X_S, the second jump n_S^* has to be compared with the value n_S that is increasing regularly with packing fraction after the first transition: once n_S and n_S^* become of equal value, no more second jump can be identified, the end point of the additional transition line has been reached.

Technically, such a cessation of a second jump is more difficult to identify precisely than a clearly developed second jump close to the crossing point, which explains the fluctuations in Fig. 3. The sharp rise in n_S around $X_S^* \approx 0.21$ has been noted before [8]. Within the results obtained here, it can be seen as a natural consequence from the crossing of a line with a finite jump in n_L and a line with a finite jump in n_S^*. For $\delta = 0.28$ [Fig. 3(b)], n_S^* and n_S merged into one line at lower X_S, suggesting that no additional transition line is found (see Fig. 1).

A comprehensive view of the evolution of the configurations of force-carrying particles including the history of the established contacts is shown in Fig. 4 for $\delta = 0.15$ and $X_S = 0.1$, as well as in the Supplemental Material videos [15] for $\delta = 0.15$ and $X_S = 0.1, 0.15, 0.19$, and 0.21, respectively. In the left column of Fig. 4, the contact-bearing large particles are shown from $\phi = 0.72$ at the first transition to $\phi = 0.871$ and $\phi = 0.875$, which is slightly before and after the second transition. Little apparent changes are visible here. In contrast for the small particles, at the first transition shown in the top row of Fig. 4, only very few of the small particles are arrested by permanent contacts. Between $\phi = 0.72$ and $\phi = 0.871$, gradually more of the small particles also establish contacts and contribute to the force network. At $\phi = 0.875$ another discontinuous jump is seen, with many of the small particles becoming arrested all at once rather than gradually.

Figure 4 shows the second discontinuity well separated from the first one, as the point $\delta = 0.15$ and $X_S = 0.1$ is already far inside the jammed regime and hence comparably far away from the first line. At the same time, the point is close to the end point where the second discontinuity vanishes, and hence the discontinuity shown in Fig. 4 is rather more moderate. More drastic jumps can be seen when getting closer to the crossing at $X_S^* = 0.21$, where, in turn, the location is closer to the first line. The videos in the Supplemental Material [15], showing the evolution of the packing with increasing density along the additional line, clearly indicate different discontinuities.

The additional transition lines are a result of the decoupling of the jamming transition between large and small particles for low X_S and low δ. Such a scenario was introduced by Furnas almost a century ago [20] to predict the highest density of aggregates entering in the manufacture of mortar and concrete. This model can be evaluated
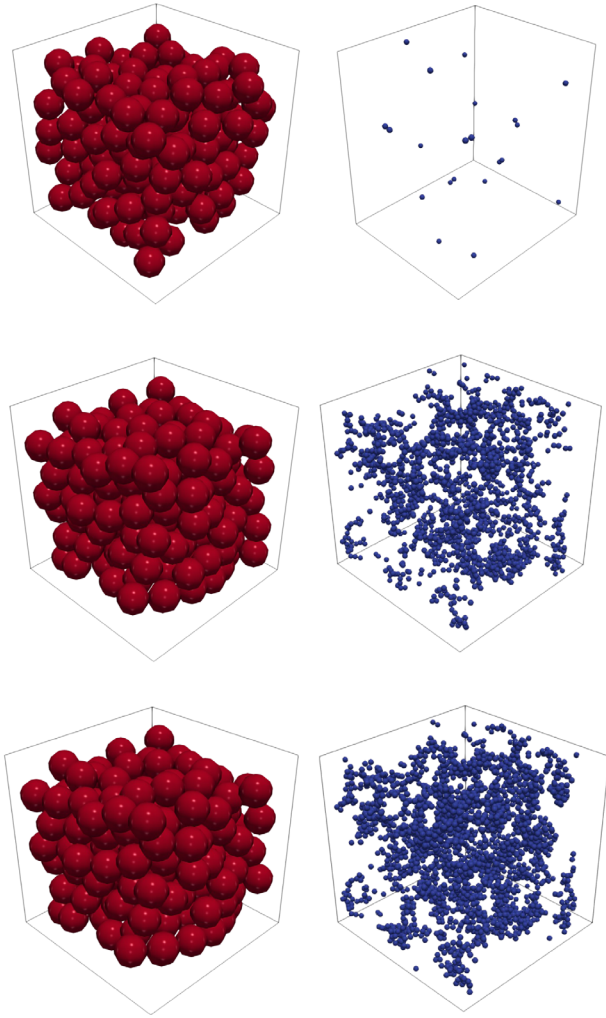
FIG. 4. Evolution of the configuration of force-carrying large (left column) and small (right column) particles for $\delta = 0.15$ and $X_S = 0.1$. The top row shows results at the transition of a loose assembly to a first force-carrying packing at $\phi = 0.72$. The middle row is shown for $\phi = 0.871$ just before the additional transition line, and the bottom row exhibits the results and configuration for the additional transition line at $\phi = 0.875$.

analytically if the size ratio of the particles is in the extreme limit $\delta \to 0$. Then, ϕ_J can be written as two lines sharing a common point at $\hat{X}_S^*$, with ϕ_{rcp} designating the packing fraction at random close packing (RCP)

$$\lim_{\delta \to 0} \phi_J(X_S) = \begin{cases} \phi_{\mathrm{RCP}}/(1-X_S), \\ \phi_{\mathrm{RCP}}/[\phi_{\mathrm{RCP}} + (1-\phi_{\mathrm{RCP}})X_S], \end{cases} \quad (1)$$

where the upper line is usually considered for $0 \leq X_S < \hat{X}_S^*$, while the lower line is deemed applicable for $\hat{X}_S^* \leq X_S \leq 1$. The other branches are usually discarded. Looking at the trend in Fig. 1 for $\delta \to 0$, one may extrapolate the simulation results to the lines given in Eq. (1). In particular,

the lower expression in Eq. (1) may in fact may be applicable for the whole range $0 \leq X_S \leq 1$.

Equation (1) predicts a line crossing with a packing fraction of $\phi_J(\hat{X}_S^*) = 0.87$ at $\hat{X}_S^* = (1-\phi_{\mathrm{RCP}})/(2-\phi_{\mathrm{RCP}}) = 0.26$, which is in reasonable agreement with the values obtained here for X_S^* at finite δ, especially when observing the upward trend in X_S^* from the simulations (cf. Fig. 1). The Furnas model then predicts an additional transition line ending at a density of unity. In Fig. 1, the additional line given by the simulation data follows qualitatively that line and ends at progressively lower values $X_S^\circ(\delta)$ for smaller δ. One may hence assume—without further proof at this point—that the extension of the Furnas formula provides a reasonable estimate for the limit of a space-filling packing within the peculiar limit where the volume of each individual small sphere vanishes with $\delta \to 0$, but where at the same time the volume contribution of the small particles remains finite for each $X_S > 0$. In the simulation for finite δ, the transition line ends at $X_S^\circ > 0$ and no discontinuity is found in n_S and Z_{SS} for $X_S < X_S^\circ$ (see Supplemental Material [15], Sec. III).

In conclusion, we have shown that the jamming diagram in bidisperse packings is enriched by an additional transition. This transition appears for $X_S < X_S^*(\delta)$ when small particles get in contact with the jammed structure already formed by large particles. The trend in the evolution of the additional line lends support to the equations of the Furnas model, which predicts a similar additional line for the intricate limit of a space-filling binary packing. The results have been obtained using a specific simulation method described above and in more detail in the Supplemental Material [15], which includes, in addition, Refs. [3,21–35], and it remains open to what extent other protocols can exhibit the same scenarios. A physical interpretation is given in order to support the reliability of the results beyond a specific protocol or implementation. Also, most notably in the simulation work in Ref. [8], parts of the findings presented here are found as well, with the exception of an additional transition line. Within a different simulation protocol and data analysis, indications of an additional transition line have been found for a mixture with $\delta = 0.17$ [35]. In addition to other computer simulations, however, the findings above should be well within the scope of experiments, e.g., along the lines of the original identification of the square-root bifurcation at jamming in two dimensions [6].

The results presented in Fig. 1 demonstrate an interesting connection to the glass-glass transition phenomenology in colloidal glasses in general [36] and binary colloidal suspensions in particular [37], thereby pointing toward a more close relationship between glass- and jamming-transition phenomena [38]: While glass and jamming transitions for hard spheres occur at different packing fractions 0.58 and 0.64 in experiments in three dimensions, they may well be considered more closely related in higher dimensions, thus allowing for a more unified description in

the future. The consideration of multiple glass as well as multiple jammed states offers the opportunity to confront theoretical concepts with richer scenarios than the correspondingly more simple transitions. Also, the relevance of different length scales in the structure of packings [39] may well reveal additional features when more than one jammed state is considered.

The extension of the jamming line found here gives a richer interpretation of the subjamming transition, a term introduced in Ref. [8]. There, the crossing point (δ^*, X_S^*) has been interpreted as showing the hallmarks of a critical point akin to those of phase transitions. From our results here we interpret this point as rather a *crossing* point of two bifurcation lines, forming part of a more general bifurcation diagram. Two jamming lines cross here, and while one terminates at the crossing, the other one can continue until its end point. This additional transition line delineates a region where small particles are inside the interstices of an already jammed structure of large particles. Increasing δ, the additional transition line shrinks, so that at some δ^*, end point and crossing point coincide, $X_S^\circ(\delta^*) = X_S^*(\delta^*)$. The scenario of Fig. 1 hence allows for the interpretation within the framework of bifurcation theory, cf. [40], where the additional line with end point can be seen as a cusp bifurcation and the whole scenario with a vanishing cusp at some point a swallowtail singularity. Also, while the existence of these bifurcations can be considered a topologically robust phenomenon, the additional line may not necessarily emerge at the maximum in packing fraction for the respective jamming-transition curves. The outline of such scenarios based on the results above should stimulate developments in theory where the analogy with phase transitions as in Refs. [8,35] on one hand and bifurcations on the other present alternative pictures that should have consequences for theoretical predictions in the field.

---

[1] H. P. Zhang and H. A. Makse, Phys. Rev. E **72**, 011301 (2005).

[2] E. Aharonov and D. Sparks, Phys. Rev. E **60**, 6890 (1999).

[3] M. van Hecke, J. Phys. Condens. Matter **22**, 033101 (2010).

[4] R. P. Behringer and B. Chakraborty, Rep. Prog. Phys. **82**, 012601 (2019).

[5] C. S. O'Hern, L. E. Silbert, A. J. Liu, and S. R. Nagel, Phys. Rev. E **68**, 011306 (2003).

[6] T. S. Majmudar, M. Sperl, S. Luding, and R. P. Behringer, Phys. Rev. Lett. **98**, 058001 (2007).

[7] A. Donev, S. Torquato, F. H. Stillinger, and R. Connelly, J. Appl. Phys. **95**, 989 (2004).

[8] I. Prasad, C. Santangelo, and G. Grason, Phys. Rev. E **96**, 052905 (2017).

[9] A. B. Hopkins, Y. Jiao, F. H. Stillinger, and S. Torquato, Phys. Rev. Lett. **107**, 125501 (2011).

[10] I. Biazzo, F. Caltagirone, G. Parisi, and F. Zamponi, Phys. Rev. Lett. **102**, 195701 (2009).

[11] S. Pillitteri, G. Lumay, E. Opsomer, and N. Vandewalle, Sci. Rep. **9**, 7281 (2019).

[12] N. Kumar and S. Luding, Granular Matter **18**, 58 (2016).

[13] N. Kumar, V. Magnanimo, M. Ramaioli, and S. Luding, Powder Technol. **293**, 94 (2016).

[14] P. A. Cundall and O. D. L. Strack, Géotechnique **29**, 47 (1979).

[15] See Supplemental Material at http://link.aps.org/supplemental/10.1103/PhysRevLett.125.215501 for details of the simulation algorithms, data analysis, and movies.

[16] O. I. Imole, N. Kumar, V. Magnanimo, and S. Luding, KONA Powder Part. J. **30**, 84 (2013).

[17] N. Kumar, S. Luding, and V. Magnanimo, Acta Mech. **225**, 2319 (2014).

[18] F. Göncü, O. Durán, and S. Luding, C. R. Mécanique **338**, 570 (2010).

[19] P. K. Morse and E. I. Corwin, Phys. Rev. Lett. **119**, 118003 (2017).

[20] C. Furnas, Ind. Eng. Chem. Res. **23**, 1052 (1931).

[21] S. Luding, Powder Technol. **158**, 45 (2005).

[22] N. P. Kruyt, I. Agnolin, S. Luding, and L. Rothenburg, J. Mech. Phys. Solids **58**, 1286 (2010).

[23] O. Durán, N. P. Kruyt, and S. Luding, Int. J. Solids Struct. **47**, 2234 (2010).

[24] J. Sun and S. Sundaresan, J. Fluid Mech. **682**, 590 (2011).

[25] F. Alonso-Marroquin, S. Luding, H. J. Herrmann, and I. Vardoulakis, Phys. Rev. E **71**, 051304 (2005).

[26] C. Thornton, Particuology **8**, 119 (2010).

[27] C. Thornton and L. Zhang, Géotechnique **60**, 333 (2010).

[28] A. Thornton, T. Weinhart, S. Luding, and O. Bokhove, Int. J. Mod. Phys. C **23**, 1240014 (2012).

[29] T. Weinhart, A. R. Thornton, S. Luding, and O. Bokhove, Granular Matter **14**, 289 (2012).

[30] C. S. O'Hern, L. E. Silbert, A. J. Liu, and S. R. Nagel, Phys. Rev. E **68**, 011306 (2003).

[31] D. Koeze, D. Vågberg, B. Tjoa, and B. Tighe, Europhys. Lett. **113**, 54001 (2016).

[32] S. Luding, Granular Matter **10**, 235 (2008).

[33] C. S. O'Hern, S. A. Langer, A. J. Liu, and S. R. Nagel, Phys. Rev. Lett. **88**, 075507 (2002).

[34] H. A. Makse, D. L. Johnson, and L. M. Schwartz, Phys. Rev. Lett. **84**, 4160 (2000).

[35] Y. Hara, H. Mizuno, and A. Ikeda, arXiv:2009.01563.

[36] M. Sperl, Phys. Rev. E **69**, 011401 (2004).

[37] T. Voigtmann, Europhys. Lett. **96**, 36006 (2011).

[38] P. Charbonneau, J. Kurchan, G. Parisi, P. Urbani, and F. Zamponi, Annu. Rev. Condens. Matter Phys. **8**, 265 (2017).

[39] D. Hexner, A. J. Liu, and S. R. Nagel, Phys. Rev. Lett. **121**, 115501 (2018).

[40] V. I. Arnol'd, *Catastrophe Theory*, 3rd ed. (Springer, Berlin, 1992).